



DOI: 10.18720/MCE.98.10

The shear behavior of CFRP strengthened RC beams

R. Al-Rousan

Jordan University of Science and Technology, Irbid, Jordan

E-mail: rzalrousan@just.edu.jo

Keywords: reinforced concrete, structural strength, shear, flexural strength, fiber reinforced polymer, nonlinear, finite element analysis

Abstract. The primary objective of this paper is to study the effectiveness of using externally applied CFRP composites as a method of shear strengthening. The parameters investigated in this study included CFRP amount and distribution (i.e., sheet versus strips), bonded surface (i.e., web sheet versus U-wrap), and fiber orientation (i.e., 90° fiber direction versus 45° fiber direction). Firstly, a novel Nonlinear Finite Element Analysis (NLFEA) model is created and validated. Then, five RC beams (150×225×1500 mm) have been constructed. The overall behavior of the NLFEA beams loaded up to failure, the onset of the cracking, and crack development with increased load and ductility were described. The NLFEA results showed that externally bonded CFRP increased the shear capacity of the strengthened RC beams significantly depending on the variables investigated. The beams strengthened with 90° CFRP U-wrap sheet provided a large increase in the ultimate load carrying capacity compared to beams strengthened with 90° CFRP web strips of 50 mm width. Decreasing the spacing between the strips is also efficient, while using 45° strips rather than 90° strips does not produce a remarkable increase in the shear capacity. The externally bonded CFRP can increase the shear capacity of the beam significantly by 34–62 % than that of the control beams, depending on the variables investigated. The inclination of the primary shear crack influenced the shear strength contribution of the external strengthening. Finally, an inclusive assessment of the NLFEA results, as well as three other well-known shear strength models, is conducted using a large test database. It is shown that the proposed shear strength, Chen and Teng, and the Chen et al. models give consistently good correlation with test data with an acceptable coefficient of variation as well as ACI Model shows unsatisfactory performance probably owing to its empirical nature and the use of an inappropriate model for the effective FRP bond length.

1. Introduction

A significant portion of the infrastructure in the world is in urgent need of strengthening and rehabilitation. Rehabilitation of either structural members or whole structures is applied when increasing live load is essential or in order to treat a structural or environmental defects. Public funds for infrastructure rebuilding are extremely limited. Therefore, engineers have been looking for innovative solutions that reduce the costs associated with traditional methods. The strengthening should be designed with consideration to minimize the maintenance and repair needs. Due to the different advantages and drawbacks of existing methods, designers must closely evaluate all of the alternatives including the possibility that strengthening may not be the best choice. Finally, it is not only the economical and structural aspects that should form the basis for decisions of strengthening and choice of strengthening method, but environmental and aesthetic aspects must also be considered. In design, the consequences from loss of strengthening effectiveness by fire, vandalism, collision should be considered as a main parameter in the external strengthening of damaged structures.

Upgrading of design standards, deterioration of the infrastructures coupled with the damage caused by natural disasters, and increased safety requirements, necessitate the need for effective construction materials for repair and strengthening of existing structure. Therefore, externally bonded carbon fiber reinforced polymer (CFRP) composites become a commonly used technique, allowing simple repair or reinforcement of structural elements, damage or otherwise structurally inadequate for verity of reasons [1–20]. The use of CFRP composites in rehabilitating structures can greatly reduce maintenance requirements, increase life safety, and increase service life of concrete structures. So far, the majority of research and applications carried out, using CFRP as strengthening material, has be devoted to use for flexural strengthening. A reinforced concrete beam



must be designed to develop its full flexural strength to insure a ductile flexural failure mode under extreme loading. Hence, a beam must have a safety margin against other types of failure that are more dangerous and less predictable than flexural failure. Shear failure of reinforced concrete beam is a type of failure mode which has a catastrophic effect, should it occur. If reinforced concrete beam deficient in shear strength is overloaded, shear failure may occur suddenly without advance warning of distress; while a flexural failure occurs gradually (if the beam is under reinforced), with large deflections and cracking giving ample warning. Also, shear failure reduces the strength of structural elements below the flexural capacity and considerably reduces the ductility of the elements. Therefore, reinforced concrete beams must have sufficient protection, strengthened, in shear zone to insure ductile flexural failure. Among FRP types, CFRP has the advantage of exhibiting relatively higher tensile strength and excellent fatigue properties. FRP reinforcement is essential for strengthening members subjected to bending, shear and can provide confinement to compression members. Structural deficiencies in reinforced concrete (RC) members can be either flexural or shear; however, shear deficiencies are inherently more dangerous because shear failures can occur suddenly and with no possibility for redistribution of internal forces. Therefore, this can be eliminated by promoting flexural failure to increase the probability of ductile flexural failure rather than brittle shear failure. Shear problems exist from insufficient design, reduction in shear reinforcement (RFT) due to corrosion or due to increase in live loads. It was evident that externally bonded FRP reinforcement can increase shear capacity in such situations [21–25]. It is evident that the ultimate resistance of FRP strengthened RC beams depends basically on the tensile strength of FRP material, FRP shear reinforcement ratio, the configuration of FRP materials and its relation to shear cracks inclinations, the compressive strength of concrete, the yield strength of shear reinforcement, the yield strength of main bars and its tensile reinforcement ratio. The shear reinforcement of strengthened RC structures by externally bonded FRP has been reported in a number of studies [26–28]. Until now, there have been a number of analytical models that describe the shear behavior of strengthened RC beams [29–34]. In general, ultimate shear capacity of strengthened RC beams proposed by these models was based on a combination of three basic elements. The first is the contribution of concrete strength, the second is the contribution of shear steel reinforcement and the third is the contribution of FRP reinforcement materials.

Although there is a tremendous effort considering the experimental works for testing RC beams strengthened with FRP sheets [1–3], there are a few experimental takes into account the effect of different strengthening configurations and parameters. Shbeeb et al. [35] studied the effectiveness of using externally bonded carbon-fiber-reinforced polymer composite sheets as a method of increasing the shear strength of reinforced concrete beams. The investigated parameters were the amount and distribution of the composite, the bonded surface and fiber orientation. The overall behavior of the test beams up to failure, the onset of cracking and crack development with increased load and ductility were recorded. Thus, the shear behavior of an RC beam in practice is more complex and difficult to understand than its behavior in flexural, although much more research has been carried out on the shear mode of failure. Therefore, Nonlinear Finite Element analysis (NLFEA) work was firstly validated against the experimental load deflection behavior and mode of failure and then the objective of this study expanded to investigate the effect of studied parameters (CFRP amount and distribution, bonded surface, and fiber orientation) on crack inclination, crack opening behavior, concrete compressive strain, and steel tensile strain.

2. Methods

NLFEA is an important and effective tool in the analysis of complex structures. The main benefits that NLFEA provided include: 1) substantial savings in the cost, time, and effort compared with the fabrication and experimental testing of structure elements; 2) allows to change any parameter of interest to evaluate its influence on the structure, such as the compressive strength of concrete; 3) allows to see the stress, strain, and displacement values at any location and at any load level; 4) the ability to change any parameter of interest, and the capability of demonstrating any interesting behavior at any load value and at any location in the system. Six full-scale models strengthened using CFRP are developed to carry out different investigated parameters.

2.1. Beam Description

The validation process of the finite element model is based on the experimental work performed by Shbeeb et al. [35]. Six rectangular reinforced concrete beams, 150 mm (width)×225 mm (depth) with a total length of 1500 mm, were cast with the reinforcement of 2×8 bars at the top and 3×15 bars. Stirrups were placed at 250 mm center to center to allow easier positioning of flexural reinforcement and to provide improved confinement of concrete along the entire beam length as shown in Fig. 1. The design choices were made to ensure that shear failure would occur in the beams. One beam was tested as control beams without strengthening and five beams were strengthened with different schemes with CFRP strips and sheets (Fig. 1). Fig. 1 shows the reinforcement and the CFRP sheet and strips configurations for all the beams specimens. All specimens were tested as simply supported in a special designed built-up rigid steel frame. A hydraulic jack was used to apply a concentrated load through a hydraulic cylinder on a spread steel beam to produce two-

point loading condition to generate a constant moment region at mid-span. Table 1 shows the failure load from the tested [35] and NLFEA.

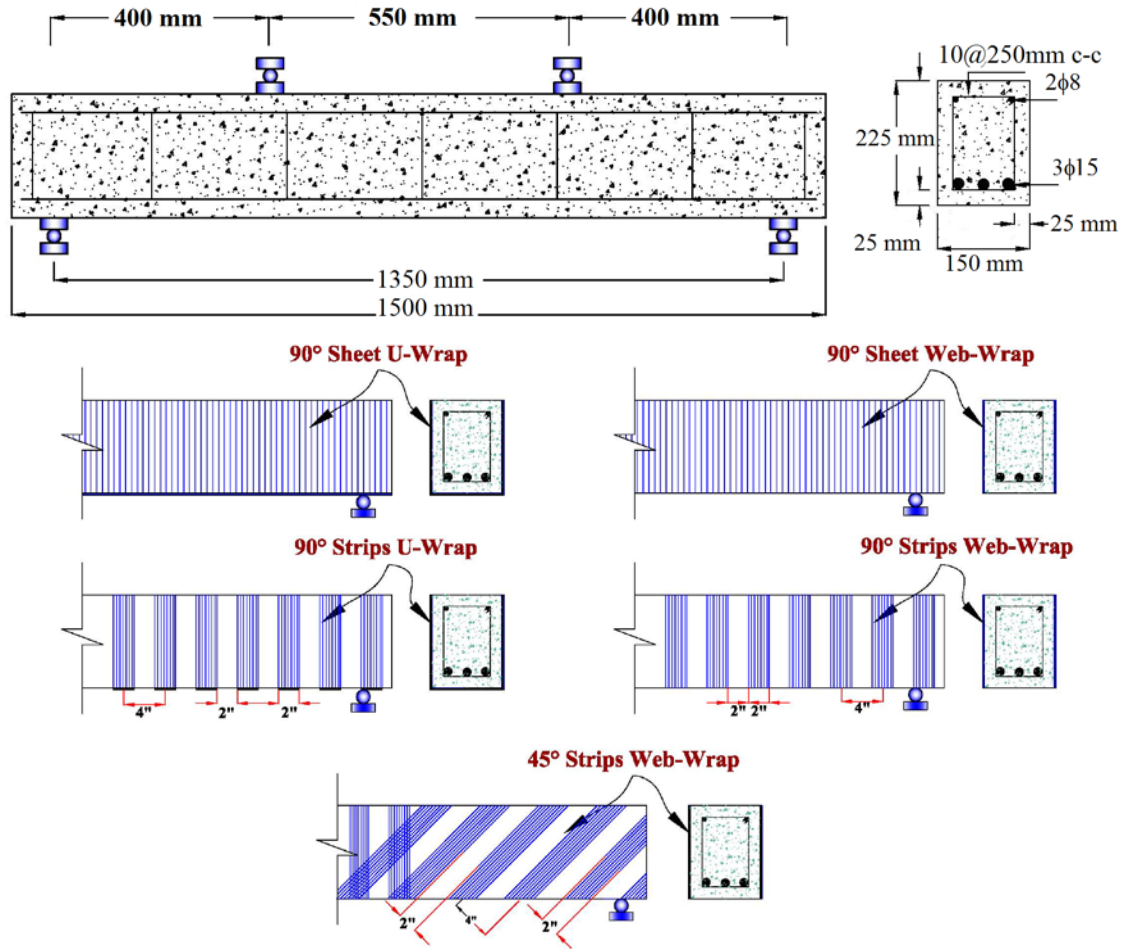


Figure 1. Setup and reinforcement details of the beams [35].

Table 1. NLFEA results.

Beam Designation	Type of strengthening	NLFEA Ultimate load, kN	Experimental. Ultimate load, kN	Percentage of increase with respect to control beam (%)
B2.2N0	Without	180.2	181.3	0
B2.2U90SH1	CFRP 90o Sheet U-Wrap	289.8	293.1	62
B2.2W90SH1	CFRP 90o Sheet Web-Wrap	261.9	264.2	46
B2.2U90ST1	CFRP 90o Strips U-Wrap	266.6	268.7	48
B2.2W90ST1	CFRP 90o Strips Web-Wrap	241.1	243.8	34
B2.2W45ST1	CFRP 45o Strips Web-Wrap	252.3	254.0	40

2.2. Description of Non-linear Finite Element Analysis (NLFEA)

Concrete is a quasi-brittle material and has different behavior in compression and tension. SOLID65 element is capable of predicting the nonlinear behavior of concrete materials using a smeared crack approach. The model is capable of predicting failure for concrete materials and accounts for both cracking and crushing failures. The two input strength parameters, ultimate uniaxial tensile and compressive strengths, are needed to define a failure surface for the concrete. Consequently, a criterion for failure of the concrete due to a multiaxial stress state can be calculated. Poisson's ratio of 0.2 was used for all beams. The shear transfer coefficient (β_t) represents the conditions at the crack face. The value of β_t ranges from 0.0 to 1.0, with 0.0 representing a smooth crack (complete loss of shear transfer) and 1.0 representing a rough crack (no loss of shear transfer). The value of β_t was used in many studies of reinforced concrete structures; however, it varied

between 0.05 and 0.25. Therefore, a value of 0.2 for β_t was used in this study. The concrete properties include concrete compressive strength of 55 MPa, initial young's modulus (E_c) of 35063 MPa. In tension, the stress-strain curve for concrete is assumed to be linearly elastic up to the ultimate tensile strength. After this point, the concrete cracks and the strength decreases to zero (Fig. 2(a)).

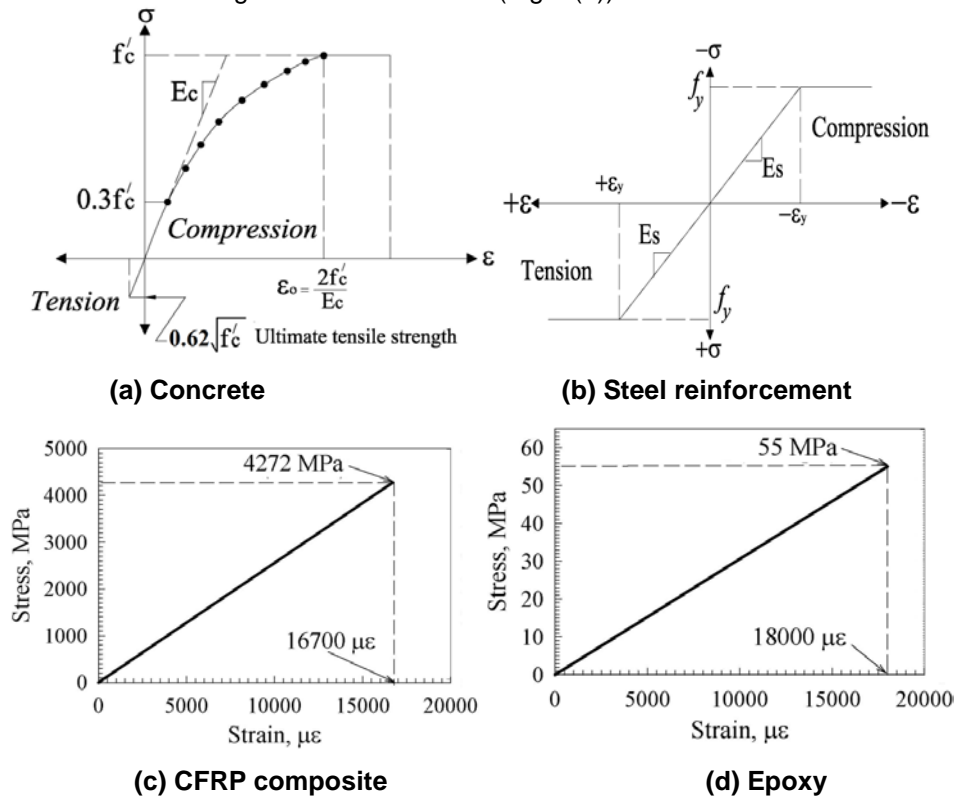


Figure 2. Stress-strain curves [35].

Fig. 2 shows the stress-strain relationships that are used in this study. The steel for the finite element models was assumed to be an elastic-perfectly plastic material and identical in tension and compression. Poisson's ratio and yield stress of 0.3 and 413 MPa respectively were used for the steel reinforcement. Fig. 2(b) shows the stress-strain relationship for steel reinforcement. Steel plates were added at both ends of the beams to provide a more even stress distribution over the support areas. The steel plates were assumed to be linear elastic materials with an elastic modulus equal to 200 GPa (29,000 ksi) and Poisson's ratio of 0.3. The CFRP composite and epoxy are modeled by a layered solid element, SOLID46. The CFRP is assumed to be an orthotropic material of 0.165 mm thick, tensile strength of 3790 MPa, elastic modulus of 228 GPa, and ultimate tensile strain of 0.017 mm/mm. The epoxy used is 0.343 mm thick, ultimate tensile strength 55 MPa, elastic modulus of 30 GPa, and ultimate tensile strain of 0.018 mm/mm. In the other directions perpendicular to the fiber direction, the elastic modulus of CFRP was assumed to be 10^{-6} times that of the main direction. Linear elastic properties were assumed for both CFRP composites and epoxy.

The total load applied was divided into a series of load increments or load steps. Newton – Raphson equilibrium iterations provide convergence at the end of each load increment within tolerance limits equal to 0.001. Load step sizes were automated by ANSYS program for the maximum and minimum load step sizes. In a concrete element, cracking occurs when the principal tensile stress in any direction lies outside the failure surface. After cracking, the elastic modulus of the concrete element is set to zero in the direction parallel to the principal tensile stress direction. Crushing occurs when all principal stresses are compressive and lies outside the failure surface; subsequently, the elastic modulus is set to zero in all directions, and the element effectively disappears. The finite element model fails impulsively when the crushing capability of the concrete is turned on. Crushing of the concrete started to develop in elements located directly under the loads. Afterward, adjacent concrete elements crushed within several load steps as well, significantly reducing the local stiffness. Finally, the model showed a large displacement, and the solution diverged. Therefore, the crushing capability was turned off and cracking of the concrete controlled the failure of the finite element models. During concrete cracking and ultimate load stages in which large number of cracks occurred, the loads were applied gradually with smaller load increments. Failure for each model was identified when the solution for 0.0045 kN load increment was not converging.

CONTA174 element was used to model the layer between the concrete and epoxy layer. This element is an 8-node element that is intended for general rigid-flexible and flexible-flexible contact analysis. In a general contact analysis, the area of contact between two (or more) bodies is generally not known in advance. Also, CONTA174 element is applicable to 3-D geometries. It may be applied for contact between solid bodies or

shells. One of the most accurate bond stress slip models that can be incorporated into a finite element analysis is that proposed by Lu et al. [36]. The mechanical behavior of the FRP/concrete interface is represented by a relationship between the local shear stress, τ , and the relative displacement, s , between the FRP composites and the concrete. Three different bond slip relations have been suggested by these authors; these are classified according to their level of sophistication and are referred to as the precise, the simplified, and the bilinear models. In the current study, the simplified model, as shown in Fig. 3, is adopted for its simplicity.

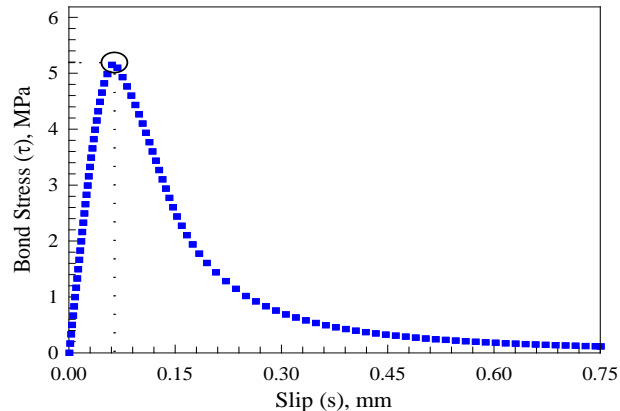


Figure 3. CFRP to concrete bond slip model [36].

Square and rectangular elements were created for the rectangular volumes (concrete, CFRP, epoxy, and steel plates) using the volume-mapped command. This properly sets the width and length of the steel reinforcement elements to be consistent with the elements and nodes of the concrete. A convergence study was carried out to determine the appropriate mesh density as shown in Fig. 4. The meshing of the reinforcement was a special case and the individual elements were created in the modeling process. However, the necessary mesh attributes for the concrete were set before each section of the reinforcement was created. SOLID46 elements for epoxy and CFRP layers had the same meshing as SOLID65 elements for concrete to allocate the node over the node of each element. The command merge item was used to merge separate entities that have the same location into single entities. To ensure proper modeling, displacement boundary conditions were applied at the planes of symmetry. The symmetry boundary conditions were set first. Nodes defining a plane through the beam cross section at the center of the beam define one plane of symmetry. The support was modeled as a roller and hinge that allows the beam to rotate at the support. The applied force was applied across the entire centerline of the steel plate. The beams were analyzed simulating 4-point loading case with the distance between the 2-point of loading is 550 mm. The total applied load was divided into a series of small load increments, each 0.45 kN, and the Modified Newton–Raphson equilibrium iterations were used to check the convergence at the end of each load increment within a tolerance value of 0.001. The static analysis type was utilized to obtain the behavior of the beams. The model failure was identified when the solution of 0.0045 kN load increment was not converging.

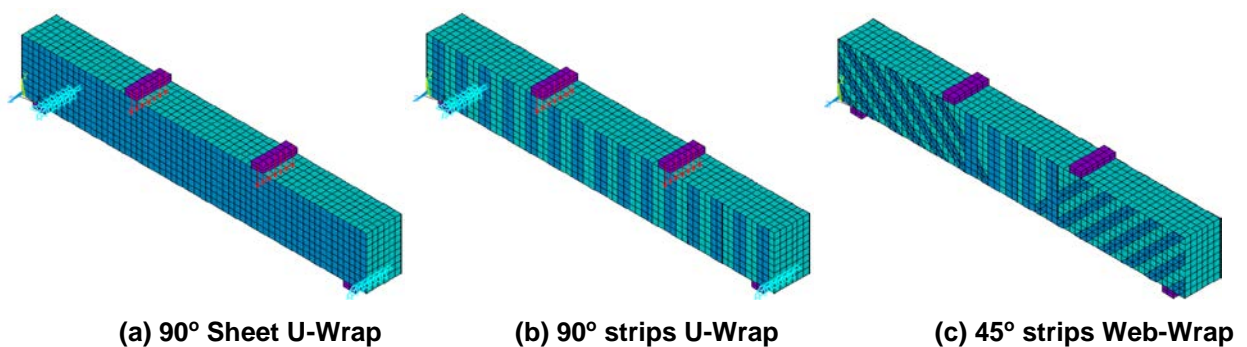


Figure 4. Typical finite element meshing of the beams.

2.3. Validation Process

Fig. 5 shows the load deflection behavior of experimental and NLFEA results. Inspection of Fig. 5 reveals that the load deflection curve can be divided into two stages: stage one represents the pre-cracking stage (creation of the first flexural crack) in which the behavior almost linear and stage two represents the after-cracking stage in which the behavior is nonlinear due to nonlinearity of concrete. With further load increase, the beams strengthened with web CFRP strips or sheet failed in shear due to debond of CFRP strips or sheet before reaching ultimate flexural capacity. The post-cracking stage was clear only for beams strengthened with CFRP 90° strips and sheet U-Wrap sloped upward indicating that the CFRP composites have a significant influence on the post-peak behavior of the strengthened beams. This could be due to the crack arresting mechanism provided by anchoring of the web strips with the tension sides of the beam.

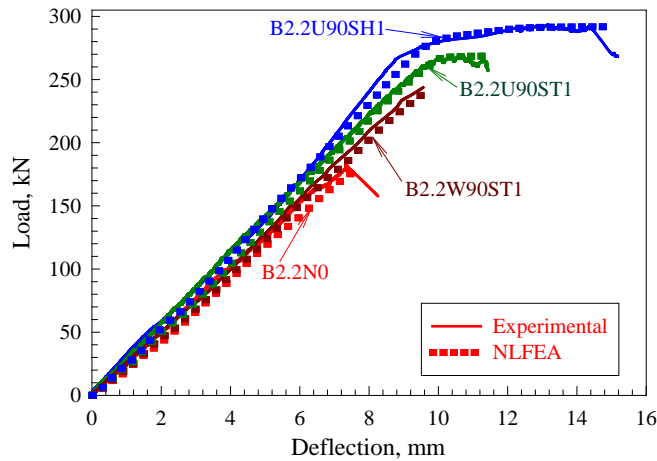


Figure 5. Experimental [35] and NLFEA load-deflection curves.

The experimental results for the tested beams are presented in Table 1. The numerical values of the ultimate strengths and the corresponding percentage increase in the ultimate shear strength of the strengthened beams over the control beam indicated that the performance of the shear deficient beams is enhanced due to the use of CFRP composites. Table 1 and Fig. 5 show that the NLFEA results correlates well with the experimental data at ultimate load capacity. Fig. 6 shows typical stress contours of the control and strengthened beams.

3. Results and Discussion

3.1. Failure Mode

Each specimen without shear reinforcement exhibited an initial flexural crack at the center of the specimen and subsequent flexural cracks away from that section. As the applied load was increased, one of the flexural cracks extended into a diagonal crack near one of the supports, or a diagonal crack formed abruptly at the mid height of the beam within the shear span area. After the formation of the diagonal crack, failure occurred by splitting along the tension reinforcement. A representative cracking pattern is shown in Fig. 6. The load carrying capacity and the mode of failure of shear reinforced concrete beams are summarized in Table 1.

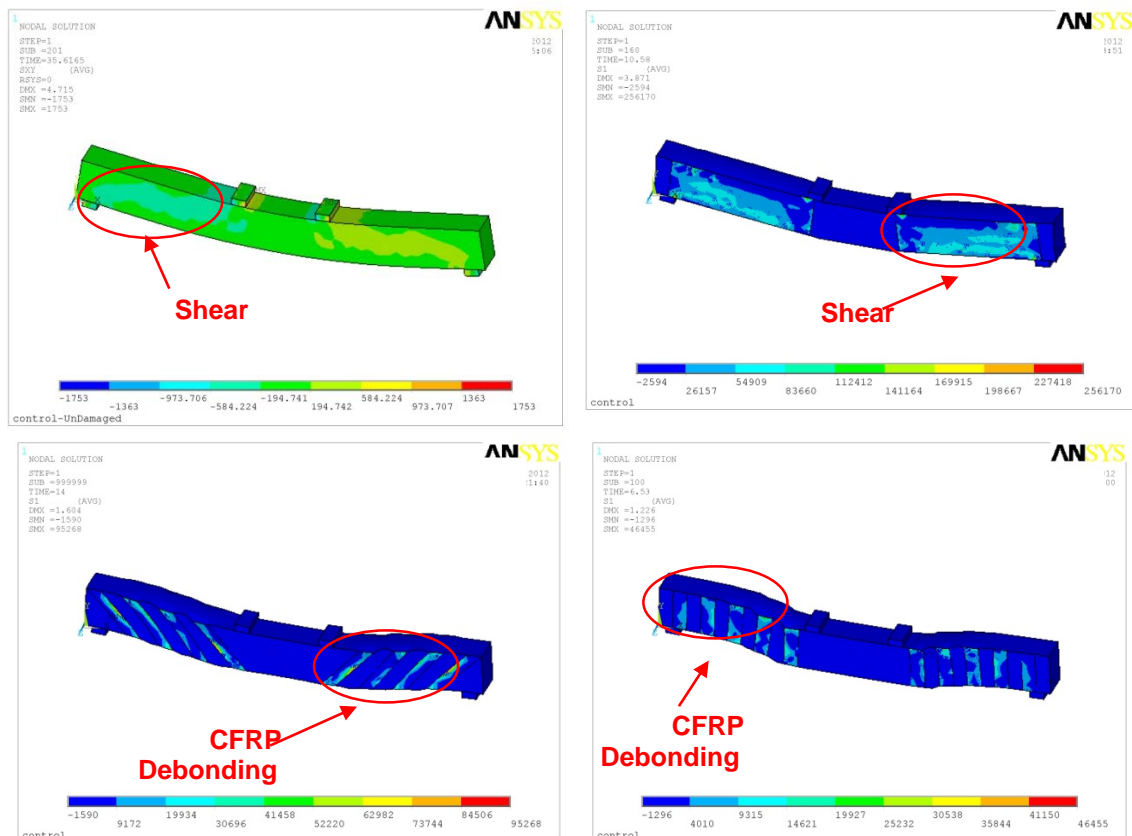


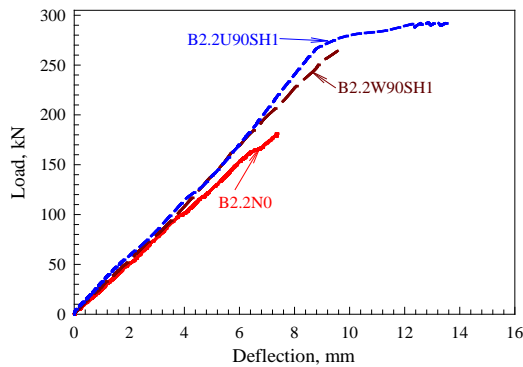
Figure 6. Typical NLFEA stress contours of NLFEA beams.

Table 2 shows the first flexural cracking load, the diagonal shear crack load, and modes of failure. The first flexural crack created within the constant moment region at a load of P_{cr} as shown in Table 2. Beyond this load, cracks extended toward the top fiber. Additional flexural cracking was developed throughout the beam length. At V_{cr} (diagonal shear crack load), a diagonal shear crack formed along a line joining the support and the load point. The crack initiated at the middle of the shear span and extended both towards the support and the load point (Table 2). All beams exhibited shear failure except CFRP 90° Sheet U-Wrap beam exhibited a ductile flexural failure and failed at a load of V_u (Table 1) as shown in Fig. 6. Finally, the shear strength increases with the increase of (1) bonded surface area (34 % for CFRP 90° Strips Web-Wrap, 40 % for CFRP 45° Strips Web-Wrap, 46 % for CFRP 90° Sheet Web-Wrap, 48 % for CFRP 90° Strips Web-Wrap, and 62 % for CFRP 90° Sheet U-Wrap); (2) CFRP distribution (48 % for CFRP 90° Strips Web-Wrap and 62% for CFRP 90° Sheet U-Wrap); and (3) CFRP orientation angle (40% for CFRP 45° Strips Web-Wrap, 46 % for CFRP 90° Sheet Web-Wrap and 48 % for CFRP 90° Strips Web-Wrap).

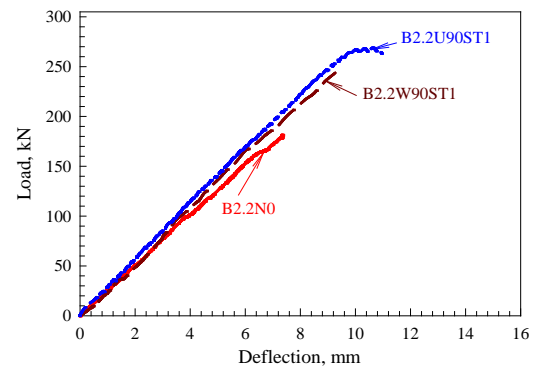
Table 2. Failure load and modes of failure.

Beam Designation	P_{cr} , kN	V_{cr} , kN	V_u , kN	Elastic Stiffness, kN/mm	Cracking stiffness, kN/mm	Failure mode
B2.2N0	32.9	115.6	180.2	27.1	20.9	Shear failure followed by 45° diagonal crack
B2.2U90SH1	34.7	133.4	289.8	28.0	25.8	Flexural failure followed by crushing of concrete in compression zone
B2.2W90SH1	34.1	211.3	261.9	25.8	23.8	Shear failure followed by 44° diagonal crack, debonding of CFRP sheets, and ripping of concrete
B2.2U90ST1	34.3	124.5	266.6	26.8	25.3	Shear failure followed by 37° diagonal crack and debonding of CFRP sheets
B2.2W90ST1	33.6	116.8	241.1	25.2	23.1	Shear failure followed by 41° diagonal crack and debonding of CFRP sheets
B2.2W45ST1	33.8	118.7	252.3	26.1	25.8	Shear failure followed by 44° diagonal crack, debonding of CFRP sheets, and ripping of concrete

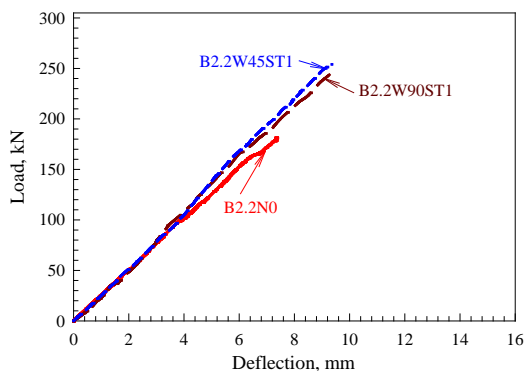
Note: P_{cr} : the first flexural cracking load, V_{cr} : the diagonal shear crack load, V_u : the ultimate shear load



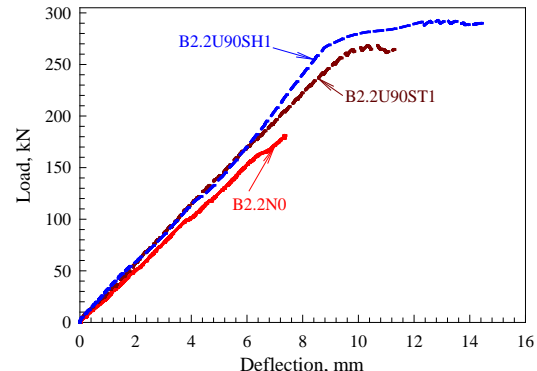
(a) Effect of bond surface (CFRP sheet)



(b) Effect of bond surface (CFRP Strips)



(c) Effect of CFRP orientation



(d) Effect of CFRP distribution

Figure 7. NLFEA load-deflection curve curves.

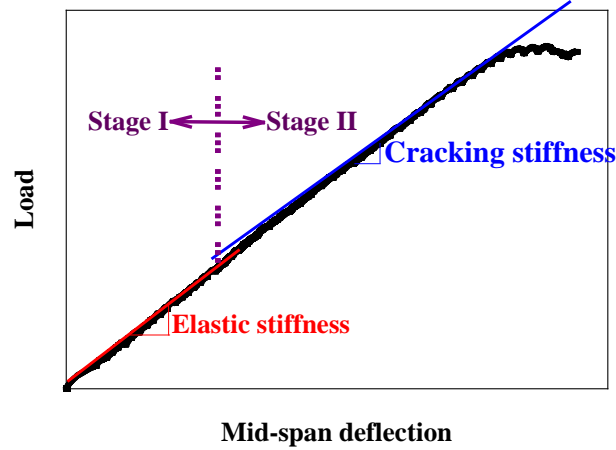
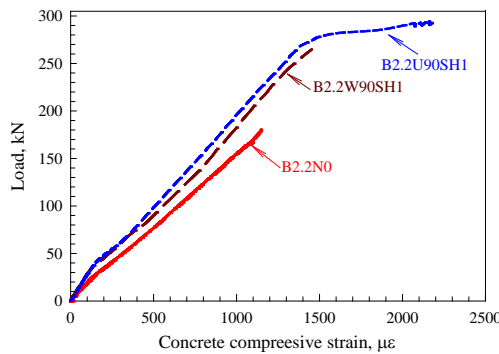


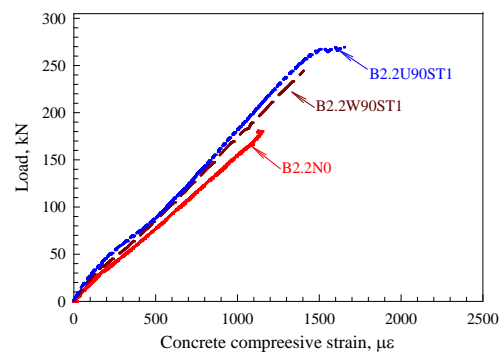
Figure 8. Stages and characteristics of load deflection behavior.

3.2. Load-deflection behavior

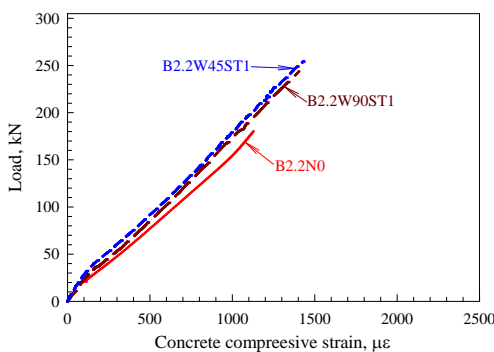
Fig. 7 shows the load deflection curves for NLFEA beams which exhibited almost linear behavior up to the load creation of the first flexural crack (P_{cr}) as shown in Table 2. The slope of the first stage of the load-deflection curve before initiation of the first main flexural crack represents the elastic stiffness while the slope of the second stage represents the cracking stiffness. This indicates that the stiffness of the beam decreased with the increase of load in which the elastic stiffness of the curve before creation of the first flexural crack is larger than the cracking stiffness as shown in Fig. 8. In addition, the increase in elastic stiffness can be observed from the angle of the diagonal shear crack (Table 2) of the elastic stage curve of the NLFEA beams in which the relationship between them is reverse. Also, the angle of the diagonal shear crack decreases with the increase of CFRP sheet bond strength area (Table 2). The load displacement curves have the same conclusion where all beams had sudden drop in load after peak load while CFRP 90° Sheet U-Wrap had ductile behavior. This indicates that an increase in the ultimate deflection can be confirmed by the use of U-wrap which give the structure behavior more ductility, and the ultimate deflection is higher than others. Inspection of Table 2 reveals that the angle of the diagonal shear crack decreases with the increase of bond surface, CFRP distribution, and CFRP sheet orientation.



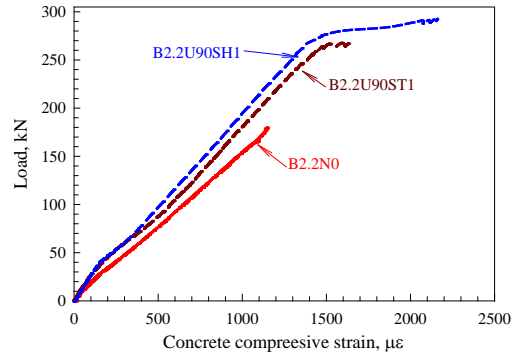
(a) Effect of bond surface (CFRP sheet)



(b) Effect of bond surface (CFRP Strips)



(c) Effect of CFRP orientation



(d) Effect of CFRP distribution

Figure 9. NLFEA load-concrete compressive strain curves.

3.3. Concrete compressive strain

Fig. 9 shows the relationship between the load and concrete compressive strain all tested beams. Inspection of Fig. 9 reveals that the compression strain increased with increasing the load as well as the concrete compressive strain in the concrete decreases with the increase of bond surface, CFRP distribution, and CFRP sheet orientation. After the yielding of steel reinforcement of B2.2U90SH1, the compression strain in concrete increased at a higher rate. The strengthened reinforced concrete beam with the U-shape CFRP sheet obtained the highest strain without occurring huge damage at the compression zone due to the confinement of the concrete.

3.4. Steel tensile strain

Fig. 10 shows the relationship between the load and strain at the level of steel for all tested beams. The load strain curve followed the same trend for all the beams before the cracking. After cracking the slope of the curve was reduced as a result of reduction in stiffness. Inspection of Fig. 10 reveals that the steel tensile strain followed the same trend and behavior as the concrete compressive strain which increased with increasing the load as well as the steel tensile strain in the concrete decreases with the increase of bond surface, CFRP distribution, and CFRP sheet orientation. B2.2U90SH1 are the only beams reached the yielding point as well as the steel reinforcement in U-shaped strengthened beam experienced highest tensile strain development than that of other beams at ultimate load.

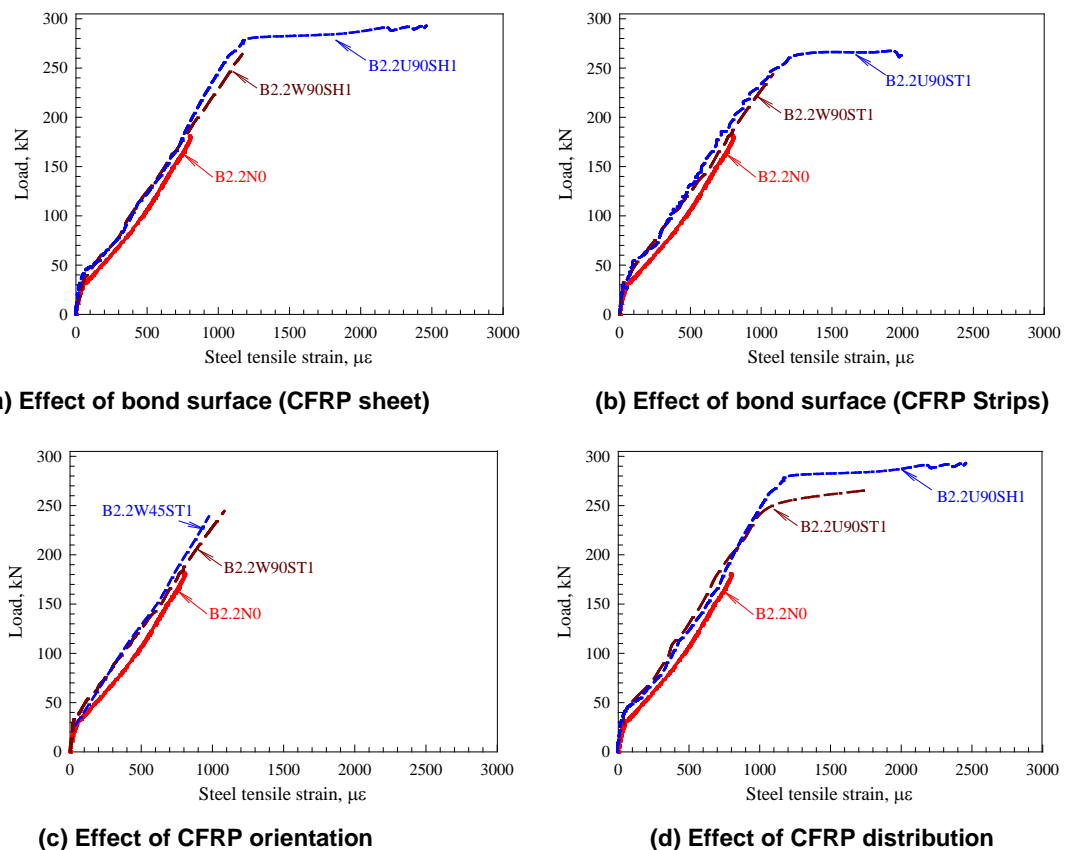
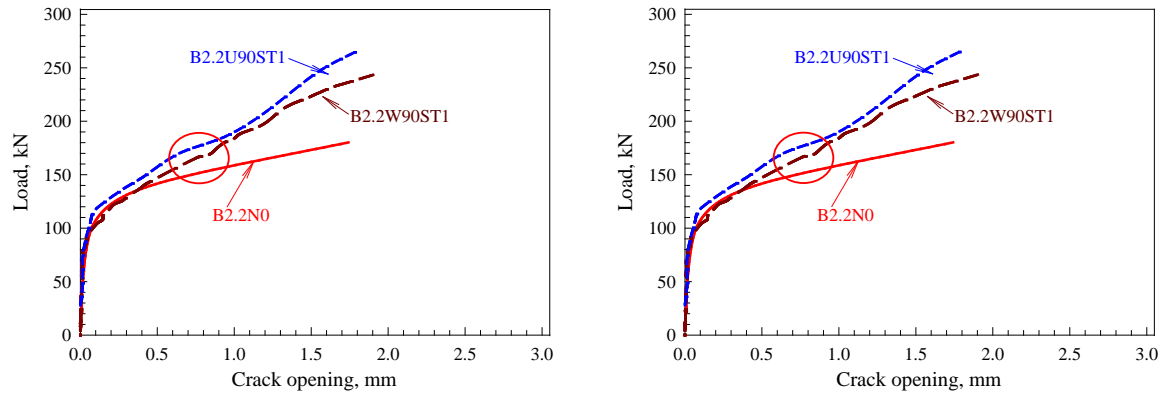


Figure 10. NLFEA load- steel tensile strain curves.

3.5. Crack opening behavior

Fig. 11 shows the relationship between the load and crack opening for beams with different CFRP strips bond surface. According to Fig. 11(a), crack opening width was initiated at load 115.7 kN and 124.5 kN for B2.2W90ST1 and B2.2U90ST1, respectively, after the formulation of diagonal shear crack. Fig. 11 shows also that the development of crack width also becomes sluggish around 0.8 mm for B2N0, B2.2W90ST1 and B2.2U90ST1. In addition, the crack width of B2N0 started to develop at 115.7 kN follows by the B2.2W90ST1 while the crack width of B2.2U90ST1 started around the load of 124.5 kN. It can be observed that the crack developed at a slower as the bond area decreases. At ultimate load, the ultimate crack width is 2.89, 1.93 and 1.82 mm for B2.2N0, B2.2W90ST1, and B2.2U90ST1, respectively. Therefore, the U-shape strengthened beam showed less crack width for the same load than the other beams. Figure 11(b) shows the relationship between the load and crack opening for beams with different CFRP orientation. According to Fig. 11(b), the development of crack width also becomes sluggish around 0.25 mm in B2.2N0, B2.2W90ST1 and B2.2W45ST1. It can be observed the crack developed at a slower rate as the CFRP orientation angle is decrease. At ultimate load, the ultimate crack width is 2.89, 1.93 and 1.07 mm for B2.2N0, B2.2W90ST1, and

B2.2W45ST1 respectively. Therefore, the 45° strips strengthened beam showed less crack width for the same load than the other beams.



(a) Effect of bond surface (CFRP Strips)

(b) Effect of CFRP orientation

Figure 11. NLFEA load-crack opening curves.

3.6. Comparison of NLFEA with theoretical models

The first step in each theoretical modeling should be adequately validated to confirm its reliability and its predictive ability against a large number of experimental of the beams with a wide range of geometrical and mechanical characteristics. These beams differ in terms of geometry, concrete strength, and amount and strength of internal and external reinforcement. The proposed model has been applied to NLFEA results as well as the literature test results. For purposes of comparison, the NLFEA results are compared with those of the Chen and Teng model [37], Chen et al. model [38], and ACI model [39]. The comparison between NLFEA and analytical results based on the proposed structural model is shown in Table 3.

Note that the ACI model was calibrated for CFRP should be used with caution for other types of composites as shown in Table 3. The overall predictions by ACI model does not appear to be equally satisfactory with a mean $V_{f,exp}/V_{f,ACI}$ value of 2.122 and a COV of 96 %. In the ACI model, the general design guidance is derived from the NLFEA data and they are only applicable to external FRP reinforcement. Based on Table 3, the proposed, Chen and Teng [37] and Chen et al. [38] models give a better prediction of NLFEA data. Therefore, Chen and Teng [37] and Chen et al. [38] models are thus applicable to all externally bonded beams irrespective of whether the bonded reinforcement is made of steel or CFRP.

Table 3. Comparison of results obtained with different models.

Beam Designation	NLFEA Ultimate load, kN	Chen and Teng model [37]	Chen et al. model [38]	ACI 440.2R model [39]
		$\left(\frac{V_{f,NLFEA}}{V_{f,mod}}\right)$	$\left(\frac{V_{f,NLFEA}}{V_{f,mod}}\right)$	$\left(\frac{V_{f,NLFEA}}{V_{f,mod}}\right)$
B2.2N0	180.2	0.941	0.951	2.078
B2.2U90SH1	289.8	0.932	0.942	2.058
B2.2W90SH1	261.9	0.980	0.990	2.163
B2.2U90ST1	266.6	0.990	1.000	2.186
B2.2W90ST1	241.1	1.000	1.010	2.208
B2.2W45ST1	252.3	0.923	0.933	2.038
Average	----	0.961	0.970	2.122
CoV (%)	----	39	39	96

4. Conclusions

1. The inclination of the primary shear crack influenced the shear strength contribution of the external strengthening.

2. The use of CFRP composites is an effective technique to enhance the shear capacity of RC beams. The externally bonded CFRP can increase the shear capacity of the beam significantly by 34 (CFRP 90° Strips Web-Wrap) to 62 % (CFRP 90° Sheet U-Wrap) than that the control beams, depending on the variables investigated.

3. Using of 45° strips rather than 90° strips does not produce a remarkable increase in the shear capacity.
4. The concrete compressive and steel tensile strain decrease with the increase of bond surface, CFRP distribution, and CFRP sheet orientation.
5. The strengthened reinforced concrete beam with the U-shape CFRP sheet obtained the highest strain without occurring huge damage at the compression zone due to the confinement of the concrete.
6. It is shown that the proposed, Chen and Teng [37] and Chen et al. [38] models give consistently good correlation with test data with an acceptable COV that can be expected for the behavior of RC beams. Therefore, Chen and Teng [37] and Chen et al. [38] models are thus applicable to all externally bonded beams irrespective of whether the bonded reinforcement is made of steel or CFRP.

References

1. Ahmed, A., Kodur, V. The experimental behavior of FRP-strengthened RC beams subjected to design fire exposure. *Engineering Structures*. 2011. 33(1). Pp. 2201–2211. DOI: 10.1016/j.engstruct.2011.03.010
2. Kodur, V.K.R., Agrawal, A. An approach for evaluating residual capacity of reinforced concrete beams exposed to fire. *Engineering Structures*. 2016. 110(1). Pp. 293–306. DOI: 10.1016/j.engstruct.2015.11.047
3. Al-Ostaz, A., Irshidat, M., Tenkhoff, B., Ponnappalli, P.S. Deterioration of bond integrity between repair material and concrete due to thermal and mechanical incompatibilities. *Journal of Materials in Civil Engineering*. 2010. 22(2). Pp. 136–144. DOI: 10.1061/(ASCE)0899-1561(2010)22:2(136)
4. Petkova, D., Donchev, T., Wen, J. Experimental study of the performance of CFRP strengthened small scale beams after heating to high temperatures. *Construction and Building Materials*. 2014. 68(1). Pp. 55–61. DOI: 10.1016/j.conbuildmat.2014.06.014
5. Ji, G., Li, G., Alaywan, W. A new fire resistant FRP for externally bonded concrete repair. *Construction and Building Materials*. 2013. 42(1). Pp. 87–96. DOI: 10.1016/j.conbuildmat.2013.01.008
6. Trentin, C., Casas, J.R. Safety factors for CFRP strengthening in bending of reinforced concrete bridges. *Composite Structures*. 2015. 128(1). Pp. 188–198. DOI: 10.1016/j.compstruct.2015.03.048
7. Ferrari, V.J., de Hanai, J.B., de Souza, R.A. Flexural strengthening of reinforcement concrete beams using high performance fiber reinforcement cement-based composite (HPFRCC) and carbon fiber reinforced polymers (CFRP). *Construction and Building Materials*. 2013. 48(1). Pp. 485–498. DOI: 10.1016/j.conbuildmat.2013.07.026
8. Attari, N., Amziane, S., Chemrouk, M. Flexural strengthening of concrete beams using CFRP, GFRP and hybrid FRP sheets. *Construction and Building Materials*. 2012. 37(1). Pp. 746–757. DOI: 10.1016/j.conbuildmat.2012.07.052
9. Kara, I.F., Ashour, A.F., Köroğ'lu, M.A. Flexural behavior of hybrid FRP/steel reinforced concrete beams. *Composite Structures*. 2015. 129(1). Pp. 111–121. DOI: 10.1016/j.compstruct.2015.03.073
10. Alver, N., Tanarlan, H.M., Sülün, Ö.Y., Ercan, E., Karcılı, M., Selman, E., Ohno, K. Effect of CFRP-spacing on fracture mechanism of CFRP-strengthened reinforced concrete beam identified by AE-SiGMA. *Construction and Building Materials*. 2014. 67(1). Pp. 146–156. DOI: 10.1016/j.conbuildmat.2014.05.017
11. Khan, A. ur R., Fareed, S. Behaviour of reinforced concrete beams strengthened by CFRP wraps with and without end anchorages. *Procedia Engineering*. 2014. 77(1). Pp. 123–130. DOI: 10.1016/j.proeng.2014.07.011
12. Hawileh, R.A., Rasheed, H.A., Abdalla, J.A., Al-Tamimi, A.K. Behavior of reinforced concrete beams strengthened with externally bonded hybrid fiber reinforced polymer systems. *Mater. Des.* 2014. 53(1). Pp. 972–982. DOI: 10.1016/j.matdes.2013.07.087
13. You, Y.-C., Choi, K.-S., Kim, J. An experimental investigation on flexural behavior of RC beams strengthened with prestressed CFRP strips using a durable anchorage system. *Composites Part B: Engineering*. 2012. 43(1). Pp. 3026–3036. DOI: 10.1016/j.compositesb.2012.05.030
14. Al-Rousan, R., Abo-Msamh, I. Bending and Torsion Behaviour of CFRP Strengthened RC Beams. *Magazine of Civil Engineering*. 2019. 92(8). Pp. 62–71. DOI: 10.18720/MCE.92.8
15. Kiyaneets, A.V. Concrete with recycled polyethylene terephthalate fiber. *Magazine of Civil Engineering*. 2018. 84(8). Pp. 109–118. DOI: 10.18720/MCE.84.11
16. Kolchunov, V.I., Dem'yanov, A.I. The modeling method of discrete cracks in reinforced concrete under the torsion with bending. *Magazine of Civil Engineering*. 2018. 81(5). Pp. 160–173. DOI: 10.18720/MCE.81.16
17. Travush, V.I., Konin, D.V., Krylov, A.S. Strength of reinforced concrete beams of high-performance concrete and fiber reinforced concrete. *Magazine of Civil Engineering*. 2018. No. 77(1). Pp. 90–100. DOI: 10.18720/MCE.77.8
18. Al-Rousan, R. Behavior of two-way slabs subjected to drop-weight. *Magazine of Civil Engineering*. 2019. 90(6). Pp. 62–71. DOI: 10.18720/MCE.90.6
19. Al-Rousan, R. The impact of cable spacing on the behavior of cable-stayed bridges. *Magazine of Civil Engineering*. 2019. 91(7). Pp. 49–59. DOI: 10.18720/MCE.91.5
20. Yu, B., Kodur, V.K.R. Fire behavior of concrete T-beams strengthened with nearsurface mounted FRP reinforcement. *Engineering Structures*. 2014. 80(1). Pp. 350–361. DOI: 10.1016/j.engstruct.2014.09.003
21. Triantafyllou, T.C., Antonopoulos, C.P. Design of concrete flexural members strengthened in shear with FRP. *J Compos Constr*. 2000. 4(4). Pp.198–205. DOI: 10.1061/(ASCE)1090-0268(2000)4:4(198)
22. Boussetlam, A., Chaallal, O. Shear strengthening reinforced concrete beams with fiber-reinforced polymer: assessment of influencing parameters and required research. *ACI Struct J*. 2004. 101(2). Pp. 219–227. DOI: 10.14359/13019
23. Belarbi, A., Bae, S., Brancaccio, A. Behavior of full-scale RC T-beams strengthened in shear with externally bonded FRP sheets. *Constr Build Mater*. 2012. 32(1). Pp. 27–40. DOI: 10.1016/j.conbuildmat.2010.11.102
24. Khalifa, A., Nanni, A. Improving shear capacity of existing RC T-section beams using CFRP composites. *Cem Concr Compos*. 2000. 22(1). Pp. 165–174. DOI: 10.1016/S0958-9465(99)00051-7
25. Mosallam, A., Banerjee, S. Shear enhancement of reinforced concrete beams strengthened with FRP composite laminates. *Composites: Part B*. 2007. 38(1). Pp. 781–93. DOI: 10.1016/j.compositesb.2006.10.002

26. Ashrafuddin, M., Baluch, M.H., Sharif, A., Al-Sulaimani, G.J., Azad, A.K., Khan, A. Peeling and diagonal tension failures in steel plated R/C beams. *Constr Build Mater.* 1999. 13(1). Pp. 459–467. DOI: 10.1016/S0950-0618(99)00044-6
27. Rangan, B.V. Shear design of reinforced concrete beams, slabs and walls. *Cem Concr Compos.* 1998. 20(1). Pp. 455–464. DOI: 10.1016/S0958-9465(98)00027-4
28. Spadea, G., Bencardino, F., Swamy, R.N. Optimizing the performance characteristics of beams strengthened with bonded CFRP laminates. *Mater Struct.* 2000. 33(1). Pp. 1119–1126. DOI: 10.1007/BF02484166
29. Malek, A.M., Saadatmanesh, H. Ultimate shear capacity of reinforced concrete beams strengthened with web-bonded fiber-reinforced plastic plates. *ACI Struct J.* 1998. 95(4). Pp. 391–399. DOI: 10.14359/555
30. Triantafillou, T.C. Shear strengthening of reinforced concrete beams using epoxy-bonded FRP composites. *ACI Struct J.* 1998. 95(2). Pp. 107–115. DOI: 10.14359/531
31. Khalifa, A., Nanni, A. Improving shear capacity of existing RC T-section beams using CFRP composites. *J Cem Concr Compos.* 2000. 22(2). Pp. 165–174. DOI: 10.1016/S0958-9465(99)00051-7
32. Hutchinson, R.L., Rizkalla, S.H. Shear strengthening of AASHTO bridge girders using carbon fiber reinforced polymer sheets. *ACI Special Publications (SP-188)*. 1999. 188(1). Pp. 945–958. DOI: 10.14359/5692
33. Zhang, Z., Hsu, C.T. Shear strengthening of reinforced concrete beams using carbon-fiber-reinforced polymer laminates. *J Compos Constr.* 2005. 9(2). Pp. 158–169. DOI: 10.1061/(ASCE)1090-0268(2005)9:2(158)
34. Monti, G., Liotta, M.A. Tests and design equations for FRP-strengthening in shear. *Constr Build Mater.* 2007. 21(24). Pp. 799–809. DOI: 10.1016/j.conbuildmat.2006.06.023
35. Shbeeb, N.I., Al-Rousan, R., Issa, M.A., Al-Salman, H. Impact of bonded carbon fibre composite on the shear strength of reinforced concrete beams. *Proceedings of the Institution of Civil Engineers: Structures and Buildings.* 2018. 171(5). Pp. 364–379. DOI: 10.1680/jstbu.16.00145
36. Lu, X.Z., Teng, J.G., Ye, L.P., Jiang, J.J. Bond–slip models for FRP sheets/plates bonded to concrete. *Engineering Structures Journal* 2005. 27(1). Pp. 920–937. DOI: 10.1016/j.engstruct.2005.01.014
37. Chen, J.F., Teng, J.G. Shear capacity of FRP strengthened RC beams: FRP debonding. *Construction and Building Materials.* 2003b. 17(1). Pp. 27–41. DOI: 10.1016/S0950-0618(02)00091-0
38. Chen, G.M., Teng, J.G., Chen, J.F. Shear strength model for FRP-strengthened RC beams with adverse FRP-steel interaction. *Journal of Composites for Construction, ASCE.* 2013. 17(1). Pp. 50–66. DOI: 10.1061/(ASCE)CC.1943-5614.0000313
39. ACI Committee 440. *Design and Construction of Externally Bonded FRP Systems for strengthening Concrete Structures.* *ACI440.2R-02. 2002. American Concrete Institute, Farmington Hills, Mich.: 45 pp. DOI: 10.1061/40753(171)159

Contacts:

Rajai Al-Rousan, rzalrousan@just.edu.jo